Environmental Monitoring using Autonomous Aquatic Robots: Sampling Algorithms and Experiments

Mahdi Jadaliha and Jongeun Choi, *Member, IEEE*

***Abstract*—This brief presents a practical solution to a problem of monitoring an environmental process in a large region by a small number of robotic sensors. Optimal sampling strategies are developed, taking into account the quality of the estimated environmental field and the lifetime of the robotic sensors. We also present experimental results for monitoring a temperature field of an outdoor swimming pool sampled by an autonomous aquatic surface robot. Simulation and experimental results are demonstrated to validate the proposed scheme.**

I. Introduction

Mobile sensor networks can be greatly exploited to monitor environmental variables such as temperature, pH, salinity, toxins, and chemical plumes. Significant enhancements have been made in the area of mobile sensor networks and their applications to environmental sciences [1], [2], [3], [4], [5], [6], [7], [8]. Decentralized environmental modeling by mobile sensor networks was presented in [1] in which control laws were developed for mobile sensors to maximize their sensory information. Planning of continuous paths for mobile sensors to reduce uncertainty in the long-term forecast was addressed in [2]. The space-time Kalman filter was proposed in [9] and utilized in [3] to model the environmental field and design distributed swarm intelligence for robotic sensors. A tradeoff between the amount of information contained in the measurements and the energy costs of acquiring the measurements was formulated in [8]. Successful implementation of optimal ocean sampling by mobile sensor networks was reported in [6]. In [7], networked unmanned autonomous aquatic surface vessels for environmental monitoring were designed and tested.

In modeling a time-varying, environmental scalar field (or a spatio-temporal process), a finite set of basis functions is often used [1], [3], [4], [9] so that a scalar value $\mu(\nu, t)$ at position ν and time t can be represented by

$$\mu(\nu, t) = \sum_{j=1}^{n_x} \psi_j(\nu) x_j(t) = \psi^T(\nu) x(t), \tag{1}$$

where $\{\psi_j(\nu)\}$ is a finite set of basis functions and $x(t)$ is a time-varying coefficient vector, which is modeled by a linear time-invariant (LTI) system driven by a stochastic input w_1

$$\frac{dx(t)}{dt} = Ax(t) + w_1(t). \tag{2}$$

In the absence of a good dynamical model of $x(t)$, often an integrator is chosen for each coefficient for the stochastic noise input [8].

In contrast to [1], [3], [4], when a small number of mobile sensing robots monitor a possibly unstable environmental process in a large surveillance region, several important problems arise. One of them is how to design a sampling strategy for robotic sensors such that a good quality of the estimation is always being maintained. On the other hand, the lifetime of the robotic sensor network has to be maximized for this resource-constrained scenario. Motivated by the aforementioned issues, this brief presents a practical solution to the environmental monitoring problem in a large region by a small number of robotic sensors and its experimental validation.

The contributions of the brief are as follows. A Kalman filter (KF) for the down-sampled environmental process has been formulated with the motivation of dynamic coverage of the surveillance region by a small number of robots in order to use the cumulative measurements over a time period. We formulated optimization problems for prediction algorithms to improve the quality of the estimation of a time-varying scalar field as well as the lifetime of a network of robotic mobile sensors due to the mobility cost. Using the down-sampled system with periodic sampling, we also provided a way to solve the formulated problems off-line for the infinite horizon. From the formulated optimization problem, we showed that there is a trade-off between the quality of the estimation and the lifetime of the robotic sensors due to the mobility cost.

This paper is organized as follows. In Section II, we introduce a spatio-temporal process using a network of radial basis functions whose coefficients follow a continuous-time linear system. A down-sampled system is formulated for a small number of robotic sensors in Section III. A KF of the down-sampled system and conditions for the discrete algebraic Riccati equation (DARE) have been discussed in Section IV. Optimal sampling strategies have been developed in Section V. Finally, in Section VI, we present experimental results for monitoring a temperature field of an outdoor swimming pool by an autonomous aquatic surface robot.

The notation throughout the paper is standard. Let $\mathbb{R}, \mathbb{R}_{\geq 0}$, and $\mathbb{Z}_{>0}$ denote, respectively, the sets of real numbers, non-negative real numbers, and positive integers. The positive

Mahdi Jadaliha is with the Department of Mechanical Engineering, Michigan State University, East Lansing, MI 48824, USA. E-mail: jadaliha@msu.edu.

Jongeun Choi is with the Department of Mechanical Engineering and the Department of Electrical and Computer Engineering, Michigan State University, East Lansing, MI 48824, USA. E-mail: jchoi@egr.msu.edu.

definiteness (positive semi-definiteness, respectively) of a matrix M is denoted by $M \succ 0$ ($M \succeq 0$, respectively). $\mathbb{E}$ denotes the expectation operator. Let $\|x\|$ denote the standard Euclidean norm (or 2-norm) of a vector x. A block diagonal matrix whose diagonal entries are given by a set of matrices $(M_1, \cdots, M_n)$ starting from the top left corner is denoted by $\text{diag}(M_1, \cdots, M_n)$. For column vectors $v_a \in \mathbb{R}^a$, $v_b \in \mathbb{R}^b$, and $v_c \in \mathbb{R}^c$, $\text{col}(v_a, v_b, v_c) := \begin{bmatrix} v_a^T & v_b^T & v_c^T \end{bmatrix}^T \in \mathbb{R}^{a+b+c}$ stacks all vectors to create one column vector. $I_n \in \mathbb{R}^{n\times n}$ denotes an $n \times n$ identity matrix. The square-root factorization for a matrix $O \succeq 0$ is defined by $O = O^{1/2}{O^{1/2}}^T$. A matrix will be called Schur if all of its eigenvalues lie strictly inside the unit disk in the complex plane. Other notation will be explained in due course.

II. Dynamical Environmental Scalar Fields

Let $Q \in \mathbb{R}^2$ be the surveillance region of interest. Suppose that the scalar field $\mu(\nu, t)$ at position $\nu \in Q$ and time $t \in \mathbb{R}$ is generated by a network of radial basis functions, which is given by (1) and (2), where $\psi^T(\nu) \in \mathbb{R}^{1\times n_x}$ and $x(t) \in \mathbb{R}^{n_x \times 1}$.

The collection of Gaussian radial basis functions $\{\psi_j(\nu) \,|\, j = 1, \cdots, n_x\}$ in $\psi^T(\nu)$ is given by

$$\begin{aligned} &\psi_1(\nu) = 1, \\ &\psi_j(\nu) = \frac{1}{\beta_j} \exp\left(\frac{-\|\nu - \xi_j\|^2}{\sigma_j^2}\right), \forall j \in \{2, \cdots, n_x\}, \end{aligned} \tag{3}$$

where σ_j is the width of the Gaussian basis function and β_j is a normalizing constant. ψ_1 is associated with a global state while other basis functions are related with local states. The center locations, i.e., $\{\xi_j\}$ are assumed to be known or need to be estimated a priori.

Modeling an environmental process (i.e., the coefficients) by an LTI system as in (1) and (2) could be justified by linearizing a nonlinear system around an operating point [1], [3], [9].

For the model in (1), the selection of the correct number of basis functions is important. Using more radial basis functions may provide better resolution. However, it demands higher computational power and more modes for robots to observe. More importantly, overfitting could happen with a large number of basis functions.

The Akaike information criterion (AIC) can be used to determine the optimal number of parameters a priori, correctly avoiding overfitting [10]. Subset selection is another technique that can improve generalization capability and avoid overfitting [11].

We assume that the dynamics of the coefficient vector $x(t) \in \mathbb{R}^{n_x}$ can be modeled by a continuous-time LTI system under a stochastic noise input. In particular, the linear system of $x(t)$ is modeled by (2), where $w_1(t) \in \mathbb{R}^{n_x}$ denotes a continuous-time Gaussian white noise process with the intensity $V_u \in \mathbb{R}^{n_x \times n_x}$. Note that the continuous-time LTI system in (2) has been considered to take into account the effect of the sampling time on the quality of the estimation and the lifetime of the robotic sensors.

We assume that n_y robotic sensors are distributed over Q. Let $q_i(t) \in Q$ be the position of the i-th sensing agent at time $t \in \mathbb{R}_{\geq 0}$. Each robotic sensor will sample a noise corrupted scalar value of interest. Robotic sensors will sample the process in (1) and (2) providing sampled-data measurements

$$\begin{aligned} y(t_k) := &\left[\psi^T(q_1(t_k)), \psi^T(q_2(t_k)), \cdots, \psi^T(q_{n_y}(t_k))\right]^T \\ &\times x(t_k) + w_2(t_k) \in \mathbb{R}^{n_y}, \end{aligned} \tag{4}$$

where $\{q_i(t_k) | i = 1, \cdots, n_y\}$ are the sampling positions at t_k. $w_2(t_k) \in \mathbb{R}^{n_y}$ denotes a discrete-time Gaussian white noise process with the covariance matrix $V_2(t_k) \in \mathbb{R}^{n_y \times n_y}$.

III. A Down-Sampled System

Due to sampling with a small number of robots over a large region, we estimate the field using a set of cumulatively collected $N \times n_y$ measurements at every N-th sampling time. To this end, we consider a down-sampled system with the accumulated sampled-data measurements over a time period, which is defined by

$$y_i := \text{col}(y(Ni+1), y(Ni+2), \cdots, y(Ni+N)) \in \mathbb{R}^{Nn_y},$$

where $i \in \mathbb{Z}_{>0}$. In general, we may assume that the sampling time intervals by robotic sensors $h_k := t_{k+1} - t_k$ are not uniform. Define the state transition matrix by $\Phi(k, j) := e^{A\sum_{l=j}^{k-1} h_l}, \forall k \geq j$. Using the fact that

$$\begin{aligned} x(k+N) &= \Phi(k+N, k)x(k) + \sum_{j=k}^{k+N-1} \Phi(k+N, j+1)u(j), \\ y(k+\ell) &= C(k+\ell)\Phi(k+\ell, k)x(k) \\ &\quad + \sum_{j=k}^{k+\ell-1} C(k+\ell)\Phi(k+\ell, j+1)u(j) + w(k+\ell), \end{aligned}$$

where $C^T(k) := [\psi(q_1(t_k)) \cdots \psi(q_{n_y}(t_k))]^T$, and $u(k)$ is a discrete-time Gaussian white noise process with the following properties

$$\begin{aligned} \mathbb{E}[u(k)] =& 0, \\ \mathbb{E}[u(k)u^T(l)] =& \delta_{k,l} \int_0^{h_k} e^{A\tau} V_u e^{A^T\tau} d\tau =: \delta_{k,l} V_1(k), \end{aligned}$$

where $\delta_{k,l}$ is a Kronecker delta function given by $\delta_{k,l} = 1$ if $k = l$, otherwise 0. The measurement noise is given by a discrete-time Gaussian white noise process $w(k) := w_2(t_k)$ with

$$\mathbb{E}[w(k)] = 0, \quad \mathbb{E}[w(k)w^T(l)] = \delta_{k,l} V_2(k).$$

We obtain the down-sampled system with collective measurements

$$x_{i+1} = F_i x_i + G_i u_i, \quad \text{and} \quad y_i = H_i x_i + v_i, \tag{5}$$

where $v_i = D_i u_i + w_i$ and other associated system parameters are provided in (6) in terms of sampled dynamics of (2). Now the processes u_i and v_i in (5) are vector-valued zero-mean Gaussian white-noise processes with the following properties.

$$\mathbb{E}\begin{bmatrix} u_i \\ v_i \end{bmatrix} = 0, \quad \mathbb{E}\begin{bmatrix} u_i \\ v_i \end{bmatrix}\begin{bmatrix} u_j^T & v_j^T \end{bmatrix} = \delta_{i,j}\begin{bmatrix} Q_i & S_i \\ S_i^T & R_i \end{bmatrix},$$

$$
\begin{aligned}
&x_i := x(Ni) \in \mathbb{R}^{n_x},\\
&u_i := \mathrm{col}(u(Ni), u(Ni+1), \cdots, u(Ni+N-1)) \in \mathbb{R}^{Nn_x},\\
&y_i := \mathrm{col}(y(Ni+1), y(Ni+2), \cdots, y(Ni+N)) \in \mathbb{R}^{Nn_y},\\
&F_i := \Phi(Ni+N, Ni) \in \mathbb{R}^{n_x \times n_x},\\
&G_i := [\Phi(Ni+N, Ni+1)\, \Phi(Ni+N, Ni+2) \cdots \Phi(Ni+N, Ni+N)] \in \mathbb{R}^{n_x \times Nn_x},\\
&H_i := \mathrm{col}(C(Ni+1)\Phi(Ni+1, Ni), C(Ni+2)\Phi(Ni+2, Ni),\\
&\qquad \cdots, C(Ni+N)\Phi(Ni+N, Ni)) \in \mathbb{R}^{Nn_y \times n_x},\\
&D_i := \begin{bmatrix} C(Ni+1) & 0 & 0 \\ C(Ni+2)\Phi(Ni+2, Ni+1) & C(Ni+2) & 0 \\ \vdots & \ddots & \\ C(Ni+N)\Phi(Ni+N, Ni+1) & & C(Ni+N) \end{bmatrix} \in \mathbb{R}^{Nn_y \times Nn_x},\\
&w_i := \mathrm{col}(w(Ni+1), w(Ni+2), \cdots, w(Ni+N)) \in \mathbb{R}^{Nn_y}.
\end{aligned} \tag{6}
$$

where the formulas for $\{Q_i, S_i, R_i\}$ are given by

$$
\begin{aligned}
Q_i &= \mathrm{diag}(V_1(Ni), V_1(Ni+1), ..., V_1(Ni+N-1)),\\
S_i &= Q_i D_i^T,\\
R_i &= D_i Q_i D_i^T\\
&\quad + \mathrm{diag}(V_2(Ni+1), V_2(Ni+2), ..., V_2(Ni+N)).
\end{aligned} \tag{7}
$$

We take the standard assumption [12] on the initial state x_0, which is that x_0 is jointly Gaussian with $x_0 \sim \mathcal{N}(\bar{x_0}, \Pi_0)$, and is uncorrelated with $\{u_i\}$ and $\{v_i\}$.

IV. The Kalman Filter

The optimal estimator for this down-sampled system in (5) is the Kalman Filter (KF) [12]. First we introduce the following standard notations. $\hat{x}_{i|j}$ and $\hat{y}_{i|j}$ are the optimal estimations (or conditional expectations) of x_i and y_i given by $\{y_0, \cdots, y_j\}$. Let $e_i := y_i - \hat{y}_{i|i-1}$ be the innovation process. Let $\tilde{x}_{i|j} := x_i - \hat{x}_{i|j}$ be the estimation error. The estimation error covariance is defined by $P_{i|j} := \mathbb{E}[\tilde{x}_{i|j}\tilde{x}_{i|j}^T]$. The discrete-time KF iterations for (5) can be written in the form of predictor updates as follows,

$$
\begin{aligned}
\hat{x}_{i+1|i} &= F_i \hat{x}_{i|i-1} + K_i(y_i - H_i \hat{x}_{i|i-1}),\\
P_{i+1|i} &= F_i P_{i|i-1} F_i^T + G_i Q_i G_i^T - K_i R_{e,i} K_i^T,
\end{aligned} \tag{8}
$$

where $K_i := (F_i P_{i|i-1} H_i^T + G_i S_i) R_{e,i}^{-1}$, and $R_{e,i} := R_i + H_i P_{i|i-1} H_i^T$, and $P_{0|-1} = \Pi_0$. Due to the sampled-data measurements for the down-sampled system we have

$$
\begin{aligned}
\hat{x}_{i|i-1} &= \mathbb{E}[x(Ni)|y(0), \cdots, y(Ni)] =: \hat{x}(Ni|Ni),\\
P_{i|i-1} &= \mathbb{E}[x(Ni) - \hat{x}(Ni|Ni)][x(Ni) - \hat{x}(Ni|Ni)]^T,
\end{aligned} \tag{9}
$$

Therefore, we use the KF predictor updates in (8) for the down-sampled system to obtain the estimates of $x(Ni)$ and the estimation error covariance matrix based on the measurements $\{y(0), y(1), \cdots, y(Ni)\}$ as shown in (9).

We assume that sensing robots are loitering around the surveillance region over a time period of revolution, which is equal to the period of the down-sampled model. Hence at the end of this period, robots will have the new updated prediction of the field. If we assume that the overall sampling sequence of intervals $[t_k, t_{k+N}]$, $k \in \mathbb{Z}_{>0}$, is periodic over $[0, \infty)$, the down-sampled system in (5) becomes an LTI system with the system parameters of $\{F, G, H, Q, S, R\}$, where time-invariant $\{S, R\}$ are obtained by the fact that $\{w(k)\}$ is cyclostationary due to the periodic sampling strategy, i.e., $V_2(k) = V_2(k+N)$. In this case, the Riccati recursion from (8) can be written as

$$
\begin{aligned}
P_{i+1|i} = &FP_{i|i-1}F^T + GQG^T - (FP_{i|i-1}H^T + GS)\\
&\times (R + HP_{i|i-1}H^T)^{-1}(FP_{i|i-1}H^T + GS)^T.
\end{aligned} \tag{10}
$$

The associated discrete algebraic Riccati equation (DARE) is given by

$$
\begin{aligned}
P = &FPF^T + GQG^T - (FPH^T + GS)\\
&\times (R + HPH^T)^{-1}(FPH^T + GS)^T.
\end{aligned} \tag{11}
$$

The associated Lyapunov equation is given by

$$
F_p^T O F_p - O + H^T (R + HPH^T)^{-1} H = 0, \tag{12}
$$

where $F_p := F - KH$ and $K := (FPH^T + GS)(R + HPH^T)^{-1}$.

It can be shown (Theorem E.5.1. in [12]) that $\{F, H\}$ is detectable and $\{F^s, GQ^{s1/2}\}$, where $F^s := F - GSR^{-1}H$ and $Q^s := Q - SR^{-1}S^T$, is controllable on the unit circle if and only if the DARE in (11) has a *stabilizing solution* P for which $F_p := F - KH$ is stable and any such stabilizing solution is unique and positive-semi-definite. In addition, under the same condition of a detectable pair $\{F, H\}$ and a controllable pair $\{F^s, GQ^{s1/2}\}$ on the unit circle, it can be also shown (Theorem E.6.1. in [12]) that $\{F^s, GQ^{s1/2}\}$ is stabilizable (i.e., controllable on and outside the unit circle) if and only if the DARE has a unique positive-semi-definite solution, which is given by the maximal (and stabilizing) solution. The following sufficient convergence conditions (Theorem 14.7.1 in [12]) are useful to ensure that the covariance matrix $P_{i|i-1}$ of the Riccati recursion in (10) converges to the solution P of the DARE in (11).

Consider the Riccati recursion in (10) with a detectable pair $\{F, H\}$ and a controllable pair $\{F^s, GQ^{s1/2}\}$ on the unit circle. Let P denote the unique stabilizing solution of the DARE in (11) and $O \succeq 0$ be the unique solution of the Lyapunov equation in (12). Then, if the initial condition Π_0 is a symmetric matrix satisfying $I + {O^{1/2}}^T(\Pi_0 - P)O^{1/2} \succ 0$, $P_{i|i-1}$ converges exponentially to P.

On the other hand, convergence with an indefinite Π_0 requires $\{F, H\}$ detectable and $\{F^s, GQ^{s1/2}\}$ stabilizable (see Theorem 14.7.2 in [12]).

Note that this convergence result holds even though F is unstable as long as the sufficient convergence conditions are satisfied. The sampling strategy of robotic sensors will be designed taking into account the aforementioned conditions for the DARE and its convergent solution.

V. Optimal Sampling Strategies

Let $r = \text{col}(r_1, \cdots, r_N) \in \mathbb{R}^{2n_y N}$ denote a sampling position vector whose position entries are associated to the sampling times $t_{Ni+1}, \cdots, t_{Ni+N}$ over a period. For simplicity, we assume that the sampling time $h_k = h$ is fixed. The sampling position vector r also serves as a collection of waypoints which robotic agents track and take measurements over a period. Note that the down-sampled system parameters can be written as functions of r, i.e.,

$$\{F, G, H(r), Q, S(r), R(r)\}.$$

Let E_k and $L_k(r)$ denote, respectively, the energy content and the energy power needed to complete the sampling for a period by the k-th robotic sensor. Then the lifetime of the k-th robotic sensor is given by

$$T_k(r) = \frac{E_k}{L_k(r)}. \tag{13}$$

In optimizing the sampling strategy, we consider mixed optimization for minimizing two conflicting cost functions such as the estimation error variances at target positions in q^{target} and another one for maximizing the lifetime of the robotic sensor network. Here the set of target points is denoted by $q^{target} := \{q_j^{target} \,|\, j = 1, \cdots, n_T\}$. As a result, the sampling strategy will minimize the estimation error variances at target points and the movement cost simultaneously.

A. A Greedy Policy over a Finite Time Horizon

For a given set $\{h_k = h | k \in \mathbb{Z}_{>0}\}$ and hyperparameters for the scalar field modeled in (1), we consider the following greedy policy which minimizes the cost function during the next finite time horizon.

$$r[i] = \arg\min_{r \in DS} J^{i+1}(r), \tag{14}$$

where $r[1], \cdots r[i]$ are sampling position vectors for periods $1, \cdots, i$. DS is the set of all possible r in which $\{F, H(r)\}$ is detectable and $\{F^s(r), GQ(r)^{s1/2}\}$ is stabilizable. The cost function at iteration $i+1$ is given by

$$J^{i+1}(r) = \lambda J_1^{i+1}(r) + (1-\lambda) J_2^{i+1}(r), \tag{15}$$

where $\lambda \in [0, 1]$ is the weight factor. $J_1^{i+1}(r)$ is the estimation performance cost function defined by the averaged estimation error variances at target positions at period $i+1$ using observations up to period $i+1$. From (1) and (9), we obtain

$$\begin{aligned} J_1^{i+1}(r) =& \frac{1}{n_T} \sum_{\nu \in q^{target}} \mathbb{E}\left[(\mu(\nu) - \hat{\mu}(\nu))^2\right] \\ =& \frac{1}{n_T} \sum_{\nu \in q^{target}} \psi^T(\nu) P_{i+1|i}(r) \psi(\nu), \end{aligned}$$

where n_T is the number of target points in q^{target}. $P_{i+1|i}$ is given by the Riccati recursion in (10) as a function of r and $P_{i|i-1}$. $J_2^{i+1}(r)$ denotes the traveling energy cost function of the sensor network. Using (13), we choose the average of the inverted lifetime over robotic sensors:

$$J_2^{i+1}(r) := \frac{1}{n_y} \sum_{k=1}^{n_y} \frac{1}{T_k(r)} = \frac{1}{n_y} \sum_{k=1}^{n_y} \frac{L_k(r)}{E_k}. \tag{16}$$

For a case where the energy power is proportional to the sum of squares of the traveled distances, we have the following cost function for a single robot.

$$J_2^{i+1}(r) := \alpha \left(\frac{\|r_N - r_1\|^2 + \sum_{k=1}^{N-1} \|r_k - r_{k+1}\|^2}{Nh} \right), \tag{17}$$

where Nh is the total sampling time for a period and α is an appropriate constant. The gradient of the cost function can be used to find a local minimum to the optimization problem in (14) in each period.

B. Infinite Horizon Optimization

A mixed optimization problem for the infinite horizon can be also formulated as follows.

$$r^{opt} = \arg\min_{r \in DS} J_\infty(r), \tag{18}$$

where $J_\infty(r) := \lambda J_1(r) + (1-\lambda) J_2(r)$ and $\lambda \in [0, 1]$ is a weighting factor. $J_1(r)$ and $J_2(r)$ in (18) are defined as follows.

$$J_1(r) := \frac{1}{n_T} \sum_{\nu \in q^{target}} \psi^T(\nu) P(r) \psi(\nu),$$

where $P(r)$ is the unique solution of the DARE in (11) for given r. J_2 can be defined similarly to (16). For a single robotic sensor, we may use the same model for J_2 as in (17).

$$J_2(r) := \alpha \left(\frac{\|r_N - r_1\|^2 + \sum_{k=1}^{N-1} \|r_k - r_{k+1}\|^2}{Nh} \right). \tag{19}$$

The optimization problem in (18) can be solved using the following gradient descent algorithm projected over DS.

$$r[j+1] = \text{Proj}_{DS}\left(r[j] - \epsilon_j \nabla_r J_\infty(r[j])\right), \tag{20}$$

where $\nabla_r J_\infty(r[j])$ denotes the gradient of J_∞ at $r[j]$, and ϵ_j is the small step size to update r at iteration j. $r[j+1]$ is the projection of $(r[j] - \epsilon_j \nabla_r J_\infty(r[j]))$ onto DS in order to satisfy the conditions for the existence and uniqueness of the solution to the DARE.

However, the computation of $\nabla_r J_\infty(r)$ requires the evaluation of $\frac{\partial P}{\partial r}$, where P is the unique solution of the DARE in (11) for $r \in DS$. In what follows, we show a way to compute it by solving a series of Lyapunov equations [13], [14].

Since $r \in DS$, the DARE has a unique positive-semi-definite solution P, which is given by the maximal (and stabilizing) solution. Since the stabilizing solution of the DARE is analytic [13], P is an infinitely differentiable function of r at any point for which the DARE admits a stabilizing solution. It can be shown that we can implicitly differentiate the DARE

TABLE I
ACHIEVED COST FUNCTION VALUES FOR DIFFERENT CASES

Case	N	h	λ	$J_1(celcius^2)$	J_2^{-1} = T (hour)
1	36	5	0.3	0.43588	19.4892
2	36	5	0.5	0.30636	7.4157
3	36	5	0.7	0.27302	5.4634
4	36	10	0.5	0.37857	12.0648
5	36	2.5	0.5	0.29559	5.8864
6	48	5	0.5	0.29412	10.3252
7	24	5	0.5	0.4202	8.4984

with respect to the i-th entry of the vector r to obtain the following Lyapunov equations for all $i \in \{1, \cdots, 2n_yN\}$ [14]:

$$F_p P^{[i]} F_p^T - P^{[i]} + X + X^T = 0, \tag{21}$$

where the superscript $[i]$ denotes the partial derivative with respect to the i-th entry of r. The other parameters in (21) are as follows.

$$F_p := F - KH,$$
$$K := (FPH^T + GS)(R + HPH^T)^{-1},$$
$$X := -F_p P (H^T)^{[i]} K^T - GS^{[i]} K^T + \frac{1}{2} K R^{[i]} K^T.$$

Since F_p is Schur (or stable), each Lyapunov equation can be uniquely solved for $P^{[i]}$.

Therefore, $\nabla_r J_\infty(r)$ evaluated at $r = r_0$ can be computed by the following way:

1) Compute P from the DARE with $r = r_0$.
2) Compute $\{P^{[i]} \,|\, i = 1, \cdots, 2n_yN\}$ by solving the Lyapunov equations in (21).
3) Compute $\nabla_r J_\infty(r)$ in (20) using $\frac{\partial P}{\partial r}$.

Numerical issues related to the computational solution of the algebraic matrix Riccati equation are discussed in [15]. In particular, computing $\nabla_r J_\infty(r)$ according to the aforementioned steps has the following computational complexity. For a fixed number of robots n_y and a fixed number of target points n_T, the complexity of the first step is $O(n_x^3) + O(n_x^2 N) + O(n_x N^2) + O(N^3)$, the complexity of the second step is $O(n_x^3 N) + O(n_x^2 N^3)$, and finally the complexity of third step is $O(n_x^2 N)$. Note that this optimization is performed offline.

C. A Trade-off Between Cost Functions

In this section, we discuss some results from the optimization presented in (18) using the method we proposed in (20) and (21). Note that the optimization in (18) is nonconvex. Hence, the suboptimal solution will be obtained via the gradient algorithm in (20).

Suboptimal solutions are found under different parameters such as λ (weighting factor), h (sampling time), and N (number of samples) for a robotic sensor as seven cases shown in Table I. We have used a model for J_2 defined in (19) with $\alpha = 2sec/(m^2 \cdot hour)$.

The estimation performance cost J_1 and the energy cost J_2 in (18) are conflicting cost functions since robotic sensors need to sample many different points to improve the quality of the estimate, which requires a lot of traveling and energy dissipation. As can be seen throughout cases 1-3, a trade-off can be obtained between the conflicting cost functions J_1 and J_2, e.g., the achieved value of J_1 decreases while that of J_2 increases as λ increases.

From the results of cases 2, 4, and 5, we see that if the sampling time h decreases, the averaged estimation error variance J_1 decreases while the energy cost J_2 increases. The effect of different numbers of sampling points for a period is shown via cases 2, 6, and 7.

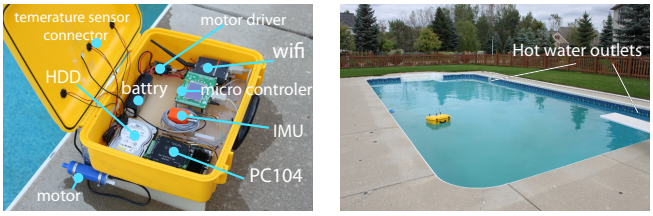

(a) (b)

Fig. 1. a) The developed robotic sensor. b) The experimental environment- a 12×6 meters outdoor swimming pool.

VI. SIMULATION AND EXPERIMENTAL RESULTS

In this section, we present experimental results using a single aquatic surface robot in an outdoor swimming pool as shown in Fig. 1. We have built our own aquatic surface robots equipped with various sensors for localization and water quality monitoring. The robot is capable of monitoring the aquatic variables in an autonomous manner while could be remotely supervised by a central station as well.

In the experimental study, we have selected and identified the system parameters based on a priori knowledge about the spatio-temporal process and sensor noise characteristics. For example, A has been chosen such that $A = -\text{diag}(0, \tau^{-1} I_{18})$, taking into account the time constant $\tau = 1000$ sec. and placing an eigenvalue at zero for $x^1(t)$ of $x(t)$ in (3) to maintain the average of the field. The system parameters for the simulation and experimental results are selected as follows: $N = 36$, $n_x = 19$, $\beta = \text{col}(1, \cdots, 1) \in \mathbb{R}^{19 \times 1}$, $\sigma = \text{col}(\infty, 2.5, \cdots, 2.5) \in \mathbb{R}^{19 \times 1}$, $h = 5$, $\lambda = 0.5$, $V_2 = 0.5 I_{36}$, $V_u = 10^{-3} I_{19}$ and $A = -10^{-3}\text{diag}(0, I_{18})$. The initial value $\Pi_0 = 2I_{n_x \times n_x}$ and $x_0 = \text{col}(10, 0, \cdots, 0) \in \mathbb{R}^{n_x}$ have been chosen for Kalman filter initial conditions. In general, the maximum likelihood estimation (MLE) using EM algorithms can be used to estimate the unknown system parameters [16]. The center locations of radial basis functions in the $12\text{m} \times 6\text{m}$ swimming pool are shown by pluses in Fig. 2-(a). The target points in q^{target} have been selected as the same as the center locations of radial basis functions.

For a comparison purpose, we have simulated the temperature field in the pool using the aforementioned system parameters. For the simulated data, the estimated temperature and the estimation error variance by our approach have been shown, respectively, in Figs. 2-(b) and (c). From (1), the estimation error variance at point q is $\mathbb{E}\left[(\mu(q) - \hat{\mu}(q))^2\right] = \psi^T(q) P_{i+1|i}(r) \psi(q)$. The counter clockwise (CCW) trajectory of simulated sampling points, which has been optimized by the proposed approach, is shown in purple solid lines with white dots for two sensor agents in Fig 2-(c). The trajectory for both agents starts from three o'clock. The true field and the

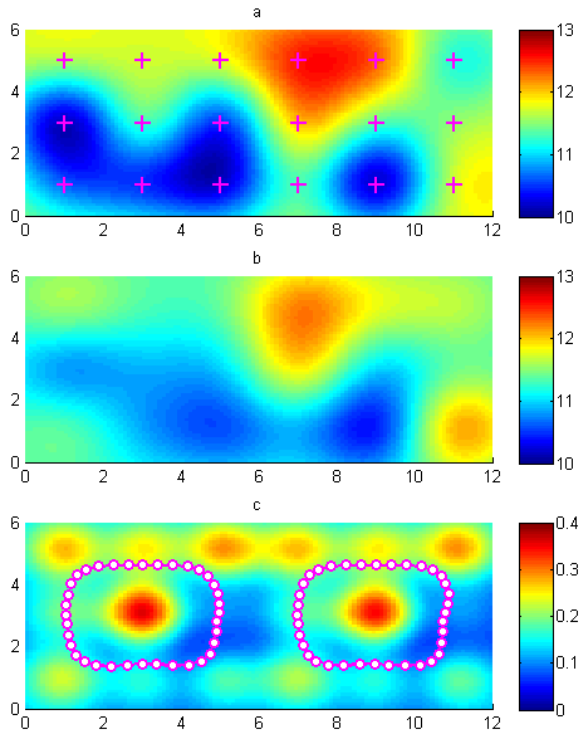

Fig. 2. (a) The simulated true temperature field. The purple pluses represent the target points and also the centers of the radial basis functions. (b) The estimated temperature field. (c) The estimation error variance field. The CCW trajectory of the simulated sampling points is shown in purple solid lines with white dots. The trajectories for both agents start from three o'clock. The axes show coordinates along horizontal and vertical directions in meters.

estimated field match well as shown in Figs. 2-(a) and (b). It is straightforward to see that the estimation error variance has been decreased in areas near the latest sampling points along the CCW sampling trajectory shown in Fig. 2-(c).

To validate our approach under an experimental setup, we control the temperature field by turning the hot water pump on and off. The hot water outlets are shown in Fig. 1-(b). We turned on the hot water pump for a while. After that, the hot water pump was turned off, and after 6 minutes, the robot collected 36 measurements in a period. The first measurement was taken at $t = 0$ sec. at a location shown as a white star in Fig. 3-(b). The estimated temperature and its error variance at $t = 175$ sec. are shown in Figs. 3-(a) and (b), respectively. Sampling points and the robot trajectory in CCW are shown, in white dots and purple solid lines in Fig. 3-(b).

The experimental setup was designed to evaluate the estimation performance of the proposed sampling strategy with one mobile robot. As can be seen in Fig. 3, there are hot spots at the left and right sides of the swimming pool. These hot spots were the result of hot water flux injected by the two hot water outlets at positions $(1, 0)$ and $(11, 0)$ in the lower-left and lower-right corners of the swimming pool, which met our expectation of high temperature around the hot water outlets, as shown in Fig. 1-(b). In addition, the estimation error variance is higher around the places where the mobile robot did not collect samples.

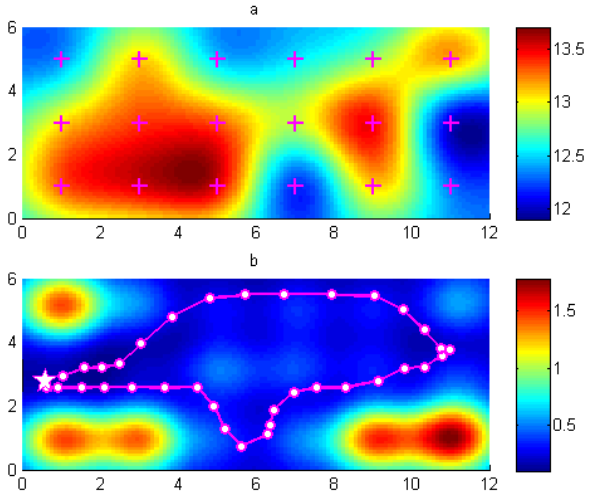

Fig. 3. (a) The estimated temperature field (in Celsius), (b) and its estimation error variance field (in Celsius^2) at time $t = 175$ sec. The first measurement point (shown with a white star) was measured in $t = 0sec$. The sampling points and the trajectory in CCW are shown with white dots and purple solid lines, respectively. The axes show coordinates along horizontal and vertical directions in meters.

VII. Conclusion

In this brief, we developed a practical solution to an environmental monitoring problem in a large region by a small number of robotic sensors. Optimal sampling strategies were developed to maximize the estimation quality and the lifetime of the robotic sensors. A trade-off between these two conflicting objectives has been presented. In addition, the effects of parameters such as the number of measurements, weighting factors, and the sampling time have been reviewed. Finally, the simulation and experimental results have been provided by our aquatic surface robot in an outdoor swimming pool with controlled hot water flux. Experimental results were demonstrated to validate the proposed scheme.

Future work will be to take into account localization errors for the estimation, and implement the experimental setup for multiple robots.

Acknowledgment

The authors thank Richard Conway for his suggestions on the optimization subject to a DARE during the 2010 DSCC conference in Cambridge, Massachusetts.

This work has been supported by the National Science Foundation through CAREER Award CMMI-0846547. This support is gratefully acknowledged.

References

[1] K. M. Lynch, I. B. Schwartz, P. Yang, and R. A. Freeman, "Decentralized environmental modeling by mobile sensor networks," *IEEE Transactions on Robotics*, 2008.

[2] H. Choi and J. How, "Continuous trajectory planning of mobile sensors for informative forecasting," *Automatica*, vol. 46, no. 8, pp. 1266–1275, 2010.

[3] J. Choi, J. Lee, and S. Oh, "Swarm intelligence for achieving the global maximum using spatio-temporal Gaussian processes," in *Proceedings of the American Control Conference*. IEEE, 2008, pp. 135–140.

[4] J. Choi, S. Oh, and R. Horowitz, "Distributed learning and cooperative control for multi-agent systems," *Automatica*, vol. 45, no. 12, pp. 2802–2814, 2009.

[5] Y. Xu, J. Choi, and S. Oh, "Mobile sensor network navigation using gaussian processes with truncated observations," *IEEE Transactions on Robotics*, vol. 27, pp. 1118–1131, 2011.

[6] N. Leonard, D. Paley, F. Lekien, R. Sepulchre, D. Fratantoni, and R. Davis, "Collective motion, sensor networks, and ocean sampling," *Proceedings of the IEEE*, vol. 95, no. 1, pp. 48–74, 2007.

[7] K. Low, G. Podnar, S. Stancliff, J. Dolan, and A. Elfes, "Robot Boats as a Mobile Aquatic Sensor Network," in *ESSA Workshop*, 2009.

[8] J. Williams, J. Fisher, and A. Willsky, "Approximate dynamic programming for communication-constrained sensor network management," *IEEE Transactions on Signal Processing*, vol. 55, no. 8, pp. 4300–4311, 2007.

[9] N. Cressie and C. Wikle, "Space-time Kalman filter," *Encyclopedia of environmetrics*, vol. 4, pp. 2045–2049, 2002.

[10] H. Akaike, "A new look at the statistical model identification," *IEEE Transactions on Automatic Control*, vol. 19, no. 6, pp. 716–723, 1974.

[11] M. Orr, "Regularization in the selection of radial basis function centers," *Neural computation*, vol. 7, no. 3, pp. 606–623, 1995.

[12] T. Kailath, A. Sayed, and B. Hassibi, *Linear estimation*. Prentice Hall NJ:, 2000.

[13] D. Delchamps, "Analytic stabilization and the algebraic Riccati equation," in *Proceedings of the IEEE Conference on Decision and Control*, vol. 22, 1983, pp. 1396–1401.

[14] R. Conway and R. Horowitz, "Analysis of Discrete-Time H2 Guaranteed Cost Performance," in *Proceedings of the ASME Dynamic Systems and Control Conference*, 2009, pp. 427–435.

[15] W. Arnold III and A. Laub, "Generalized eigenproblem algorithms and software for algebraic Riccati equations," *Proceedings of the IEEE*, vol. 72, no. 12, pp. 1746–1754, 1984.

[16] R. Shumway and D. Stoffer, "An approach to time series smoothing and forecasting using the EM algorithm," *Journal of time series analysis*, vol. 3, no. 4, pp. 253–264, 1982.